Self-organization of multiarmed spiral waves in excitable media

Benjamas Ponboonjaroenchai,[1] Jiraporn Luengviriya,[2] Malee Sutthiopad,[1] Piyachat Wungmool,[1] Nakorn Kumchaiseemak,[1] Stefan C. Müller,[3] and Chaiya Luengviriya[1,*]

[1]*Department of Physics, Kasetsart University, 50 Phaholyothin Road, Jatujak, Bangkok 10900, Thailand*

[2]*Lasers and Optics Research Group, Department of Industrial Physics and Medical Instrumentation, King Mongkut's University of Technology North Bangkok, 1518 Pibulsongkram Road, Bangkok 10800, Thailand*

[3]*Institute of Physics,Otto-von-Guericke University Magdeburg, Universitätsplatz 2, D-39106 Magdeburg, Germany*

(Received 3 December 2018; revised manuscript received 9 August 2019; published 2 October 2019)

We present an investigation of self-organized multiarmed spiral waves pinned to unexcitable circular obstacles in a thin layer of the excitable Belousov-Zhabotinsky reaction and in simulations using the Oregonator model. The multiarmed waves are initiated by a series of wave stimuli. In the proximity of the obstacle boundary, the wave rotation around the obstacle causes damped oscillations of the wave periods of all spiral arms. The dynamics of wave periods cause the wave velocities as well as the angular displacements between the adjacent arms to oscillate with decaying amplitudes. Eventually, all displacements approach approximately the same stable value so that all arms are distributed evenly around the obstacle. A further theoretical analysis reveals that the temporal dynamics of the angular displacements can be interpreted as underdamped harmonic oscillations. Far from the obstacles, the wave dynamics are less pronounced. The wave period becomes stable very soon after the initiation. When the number of spiral arms increases, the rotation of individual arms slows down but the wave period of the multiarmed spiral waves decreases. Due to their short period, multiarmed spiral waves emerging in the heart potentially result in severe pathological conditions.

DOI: 10.1103/PhysRevE.100.042203

I. INTRODUCTION

Spiral waves have been studied in various nonlinear reactive systems, for instance, in the CO oxidation on a platinum surface [1], in cell aggregation in slime mold colonies [2], as calcium waves in *Xenopus* oocytes [3], in the Belousov-Zhabotinsky (BZ) reaction [4], and as electrical spiral waves of excitation in heart tissue [5]. It is conjectured that the electrical spiral waves in heart tissue are related to tachycardia which can lead to sudden cardiac death by ventricular fibrillation [6,7]. These pathological cardiac conditions may last over a prolonged time period when the spiral waves are pinned to anatomical obstacles, e.g., blood vessels or scars [5]. Therefore, it is important to study the dynamics of pinned spiral waves in order to effectively eliminate the waves.

Unexcitable disks have been often used as obstacles to study their influence on the dynamics of spiral waves. The wave period, wavelength, and wave velocity of pinned spiral waves increase with the obstacle diameter [8–12]. Furthermore, elimination of the pinned spiral waves was also found to be affected by the obstacle size: unpinning a spiral wave from a larger obstacle required stronger external forcing including the application of a wave train [13,14] or an electrical field [15,16].

Interaction of spiral waves results in complex dynamics in excitable systems, for example, multiarmed spiral waves, which are multiple spiral waves that rotate in the same direction around a common center. Agladze and Krinsky [17] have demonstrated the creation of multiarmed spiral waves in the Belousov-Zhabotinsky (BZ) reaction where a KCl droplet was used as the obstacle. They mentioned that the multiarmed spiral waves cannot exist in real excitable systems without an obstacle. Steinbock and Müller [18] used a laser spot to create a temporary obstacle for pinning multiarmed spiral waves in a photo-sensitive BZ reaction. After the laser spot was switched off, the obstacle area became excitable and individual cores were formed for each arm.

Multiarmed spiral waves were also investigated in biological excitable media. They were formed in mounds of *Dictyostelium discoideum* by a convergence of single spiral waves located close to each other [19]. In a rabbit heart, multiarmed spiral waves appeared to be associated with the underlying anatomic structure [20]. In cardiac cell culture samples, a short and rapid train of electrical stimuli created multiarmed spiral waves rotating with a frequency higher than that of single spiral waves [21].

In this article, we present the dynamics of multiarmed spiral waves pinned to circular unexcitable obstacles in the BZ reaction by using a series of wave stimuli close to an impermeable partition. The experiments are corroborated by simulations using the Oregonator model [22]. The dynamics of waves close to and far from the obstacles are analyzed.

II. EXPERIMENTS

A. Experimental methods

The BZ reaction used in our experiments is composed of $NaBrO_3$, malonic acid (MA), H_2SO_4, and ferroin, all purchased from Merck. In addition, a small amount of surfactant,

*Corresponding author: fscicyl@ku.ac.th

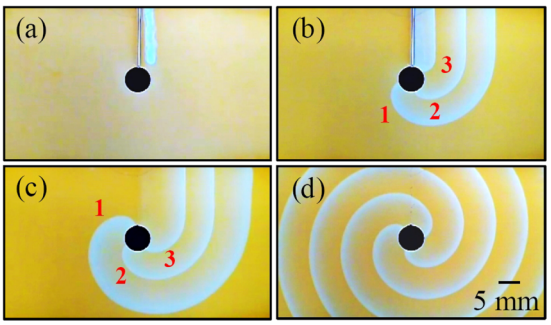

FIG. 1. Initiation of a three-armed spiral wave pinned to an obstacle in the BZ reaction. (a) A planar wave front is ignited close to the partition to create the first arm. (b) The second and third arms are generated. The labels 1, 2, and 3 depict the order of wave initiation. (c) The partition is removed to allow autonomous wave propagation. (d) After a transient interval, the forms of all arms are identical, and the distances become alike.

sodium dodecyl sulfate (SDS, from Fluka), is added to the solution to reduce the production of CO_2 bubbles, which are uncontrollable inhomogeneities. Stock solutions of $NaBrO_3$ (1 M), MA (1 M), and SDS (1 M) are freshly prepared by dissolving powder in deionized water, whereas stock solutions of H_2SO_4 (2.5 M) and ferroin (25 mM) are commercially available. Appropriate volumes of the stock solutions are mixed and diluted in deionized water to form BZ solutions with initial concentrations $[NaBrO_3] = 50$ mM, $[MA] = 50$ mM, $[\text{ferroin}] = 0.625$ mM, $[SDS] = 0.05$ mM, and $[H_2SO_4] = 160$ mM. To prevent hydrodynamic perturbations, the reaction is prepared in 0.5% agar gel.

The experiments are performed using a transparent rectangular reactor with a volume of $100 \times 50 \times 10\,\text{mm}^3$ and its top plane (area $100 \times 50\,\text{mm}^2$). It is in contact with a thermostating transparent bath to control the temperature at $22 \pm 1\,^\circ\text{C}$. The reactor is set between a white light source and a color CCD camera (Super-HAD, Sony) to record the images of the medium at intervals of 1 s with a spatial resolution of $100\,\mu\text{m pixel}^{-1}$.

B. Experimental results

Figure 1 demonstrates the initiation of a three-armed spiral wave using a partition method. A thin rectangular glass plate and a chemically inert plastic cylinder are used as the partition and the obstacle, respectively. The obstacle (6 mm in diameter and 3 mm in height) is attached at the middle of the reactor using silicone paste [see the circle in the middle of Fig. 1(a)]. The partition is set between an inner wall of the reactor and the obstacle [see the vertical thin line in the middle of Fig. 1(a)]. A volume of 20 ml BZ solution is filled into the reactor so that the thickness of the solution layer is approximately 3–4 mm. Immersion of a silver plate into the medium (close to the partition) stimulates two planar wave fronts [thick band in Fig. 1(a)]. In the course of time, one wave front propagating towards the partition will be annihilated and the other will move away from the partition with its end contacting the obstacle. This process is repeated to initiate the second and the third wave fronts, as shown in Fig. 1(b). Subsequently, the partition is removed so that the thin line of partition disappears as shown in Fig. 1(c). Finally, the distances between the adjacent spiral arms, which are initially different, gradually become equal in the course of time; i.e., the structure follows a self-organized rotation, as shown in Fig. 1(d).

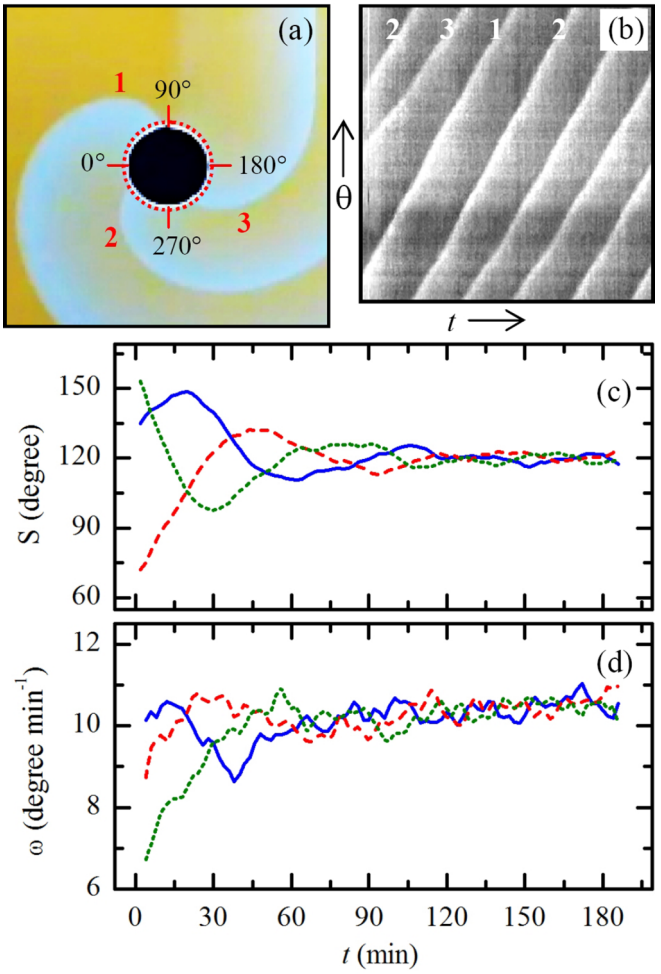

FIG. 2. Dynamics of the three-armed spiral wave. (a) Pixels along the closed loop (dashed circle) are taken to construct (b) a time-space plot (θ, t). Labels 1, 2, and 3 indicate the spiral arms in the order of initiation. (c) The angular displacements between adjacent spiral arms S_{12}, S_{23}, and S_{31} (solid, dashed, and dotted lines, respectively) and (d) the angular velocities of the spiral arms ω_1, ω_2, and ω_3 (solid, dashed, and dotted lines, respectively) are plotted as a function of time.

Figure 2 illustrates an analysis of the dynamics of the three-armed spiral waves. To elucidate the motion of the spiral fronts attached to the obstacle, we take the gray level of the pixels along a circular path close to the obstacle boundary, the dashed circle as in Fig. 2(a), to formulate a time-space plot shown in Fig. 2(b). The spiral fronts appear as bright lines in this plot. In order to quantify the distribution of spiral arms around the obstacle, we measure the angular displacement between adjacent arms as follows.

At a given time, the angular positions (θ_1, θ_2, and θ_3) of the spiral arms in the time-space plot are identified. Then the angular displacement S_{ij} between two adjacent arms i and j is calculated. S_{ij} is the counterclockwise angle from arm i to

arm j. The temporal evolution of angular displacements S_{12}, S_{23}, and S_{31} is plotted in Fig. 2(c). For better understanding of the wave dynamics, we calculate the angular velocity ω_i of each arm (ω_1, ω_2, and ω_3), which is the temporal change of the angular positions (θ_1, θ_2, and θ_3, respectively) as shown in Fig. 2(d).

The angular displacements S_{12}, S_{23}, and S_{31} [Fig. 2(c)] oscillate with damped amplitudes. These oscillations are caused by the three spiral arms rotating with angular velocities ω_1, ω_2, and ω_3 [Fig. 2(d)]. The time-dependent behavior of the angular velocities originates, in fact, from the interaction of the spiral arms. In the beginning, the first arm propagates with a high velocity since the medium has a relatively high excitability. The second arm has a lower velocity ($\omega_1 > \omega_2$) because it is moving in the wake of the first one. This also applies for the third arm so it has the lowest velocity. When the measurement started at $t = 0$ min, the displacement between arm 1 and arm 2 (S_{12}) is larger than that between arm 2 and arm 3 (S_{23}) because the relation of the velocities is $\omega_1 > \omega_2 > \omega_3$ ($10.1 > 8.7 > 6.7^\circ\,\mathrm{min}^{-1}$).

We now describe the oscillation of the displacement S_{12} that is affected by the velocities ω_1 and ω_2. Soon after the measurement starts, S_{12} increases because the first arm rotates faster than the second one ($\omega_1 > \omega_2$). When the first arm travels into the refractory tail of the third arm ($\theta_1 > 90^\circ$), its velocity ω_1 starts to decrease. S_{12} reaches a maximum at 20 min (i.e., when ω_1 and ω_2 are equal) and subsequently decreases since the first arm becomes slower than the second one ($\omega_1 < \omega_2$). After 40 min, ω_1 increases from a minimum until it equals ω_2 at 60 min, so that S_{12} reaches a minimum at this time. Then the first arm rotates again faster that the second arm ($\omega_1 > \omega_2$), so that S_{12} increases until it reaches a maximum at $t = 105$ min. The oscillation of S_{12} continues with decreased amplitude, since the difference of ω_1 and ω_2 decreases in the further course of time.

Like S_{12}, the oscillations of other displacements can be explained by considering the velocities ω_2 and ω_3 (for S_{23}) or ω_3 and ω_1 (for S_{31}). All displacements S_{12}, S_{23}, and S_{31} and velocities ω_1, ω_2, and ω_3 continually oscillate with amplitudes decaying in time. After 120 min, the three arms are distributed quite evenly around the obstacle: all angular displacements approach $120.0^\circ \pm 1.5^\circ$, and all arms rotate with a similar angular velocity of $10.5^\circ\,\mathrm{min}^{-1} \pm 0.2^\circ\,\mathrm{min}^{-1}$.

To gain a deeper understanding of the oscillations, the wave periods of the spiral arms close to the obstacle T_{obs} are derived from the time-space plot [Fig. 2(b)]. At a given instance of time, the wave period of a spiral arm is defined as the delay time between current and preceding spiral arms reaching the same position θ. Note that the positions of all spiral arms θ_1, θ_2, and θ_3, where the periods are measured, change with time since the fronts always move. Figure 3(a) shows that the wave periods of spiral arms 1, 2 and 3 ($T_{1\mathrm{obs}}$, $T_{2\mathrm{obs}}$, and $T_{3\mathrm{obs}}$) oscillate with damped amplitudes similar to their corresponding angular velocities ω_1, ω_2, and ω_3 [Fig. 2(d)]. Figure 3(b) illustrates the dispersion relation, which is a plot of all wave velocities [Fig. 2(d)] as a function of the wave periods [Fig. 3(a)]. Even though these variables are measured close to the obstacle where the wave fronts are curved, the velocity increases monotonously with the wave period, similar to earlier results for propagating plane waves in the BZ reaction [23,24]. Thus, the damped oscillations of the velocities [Fig. 2(d)] as well as the displacements [Fig. 2(d)] originate from the dispersion relation and the oscillations of the wave periods.

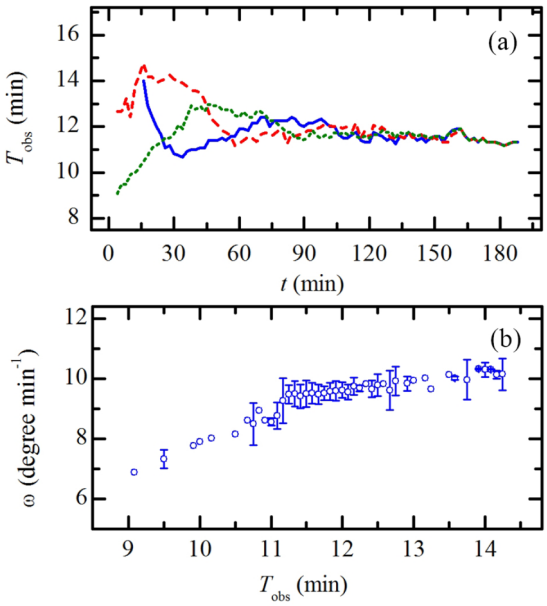

FIG. 3. (a) Time-dependent wave periods close to the obstacle T_{obs} of the spiral arms 1, 2, and 3: $T_{1\mathrm{obs}}$, $T_{2\mathrm{obs}}$, and $T_{3\mathrm{obs}}$ (solid, dashed, and dotted lines, respectively) and (b) dispersion relation of the three-armed spiral wave. Circles represent the average value of measured angular velocities corresponding to a given wave period; standard deviation indicated by bars.

To analyze the wave dynamics far from the obstacle, the wave period of the wave fronts emitted by the three-armed spiral wave is measured. We performed additional experiments to generate single-armed and two-armed spiral waves in order to investigate the effect of the number of arms on the wave period far from the obstacles. Unlike the oscillations in Figs. 2(c) and 2(d), the wave periods change monotonously at the beginning and subsequently approach stable values, as shown in Fig. 4. When the number of arms increases, the wave period decreases, i.e., the periods for the single-armed, two-armed, and three-armed spiral waves are $T_1 = 26.2$, $T_2 = 15.3$, and $T_3 = 11.6$ min, respectively. However, each of their spiral arms completes one revolution within an interval that

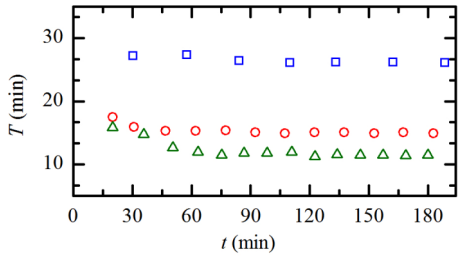

FIG. 4. The wave period of multiarmed spiral waves. It is measured far from the obstacle (i.e., at the left bottom corner in Fig. 1). Squares, circles, and triangles depict the period of single-armed, two-armed, and three-armed spiral waves, respectively.

increases with the number of arms: $T_1 = 26.2$, $2T_2 = 30.6$, and $3T_3 = 34.8$ min, and wave velocities are 1.13, 0.84, and 0.73 mm min^{-1} for the cases of one, two, and three arms, respectively. Thus, the interaction of the spiral arms via the refractory tail causes each arm to slow down.

III. SIMULATIONS

A. Simulation methods

Numerical simulations have been performed using the two-variable Oregonator model to describe the dynamics of the two variables u and v (corresponding to the concentrations of $HBrO_2$ and the catalyst, respectively, in the BZ reaction) as in Eq. (1):

$$\frac{\partial u}{\partial t} = \frac{1}{\varepsilon}\left(u - u^2 - fv\frac{u-q}{u+q}\right) + D_u\nabla^2 u,$$
$$\frac{\partial v}{\partial t} = u - v + D_v\nabla^2 v. \quad (1)$$

Parameters $\varepsilon = 0.01$, $q = 0.002$, and $f = 1.4$, and diffusion coefficients $D_u = 1.0$ and $D_v = 0.6$ are chosen as in a study by Jahnke and Winfree [25]. The variables u and v in Eq. (1) are calculated using an explicit Euler method with a nine-point approximation of the two-dimensional Laplacian operator on a discrete system with a uniform grid space $\Delta x = \Delta y = 0.1$ space unit (s.u.) and a time step $\Delta t = 3.0 \times 10^{-3}$ time unit (t.u.), as required for numerical stability [$\Delta t \leqslant (3/8)(\Delta x)^2$ [26]].

The dimensionless size of the system is 80×80 s.u. (corresponding to 800×800 grid points). To initiate multiarmed spiral waves pinned to a circular obstacle using a partition method, a series of planar waves close to the partition is triggered by setting a five-grid-point strip to an excited state ($u = 1.0$). The boundaries of the system, the partition, and the circular obstacle have no-flux conditions as described in Ref. [27].

B. Simulation results

Figure 5 shows the evolution of a simulated three-armed spiral wave pinned to an obstacle with 10.0 s.u. in diameter. After they are ignited, the three arms rotate clockwise, and their front widths are noticeably different, i.e., the following fronts become thinner [Fig. 5(a)]. When the first arm pass the line prior occupied by the partition, i.e., into the refractory tail of the third arm, its width strongly decreases [Fig. 5(b)]. Then the first arm becomes the thinnest one so that the second arm has the thickest front [Fig. 5(c)]. In this initial phase, the distances between adjacent arms are different. In the course of time, the three-armed spiral wave gradually adjusts form and distance, until all arms have the same front width and stay apart from each other at the same distance [Fig. 5(d)].

The dynamics of the simulated three-armed spiral wave are analyzed in the same manner as in the experimental part. The gray level of the pixels on a circle close to the obstacle boundary, as shown in Fig. 6(a), are taken to construct a time-space plot [Fig. 6(b)] in which the spiral fronts appear as dark lines. At a given time, the angular positions (θ_1, θ_2, and θ_3) of the spiral arms are identified, and the angular displacements (S_{12}, S_{23}, and S_{31}) between two adjacent arms are calculated.

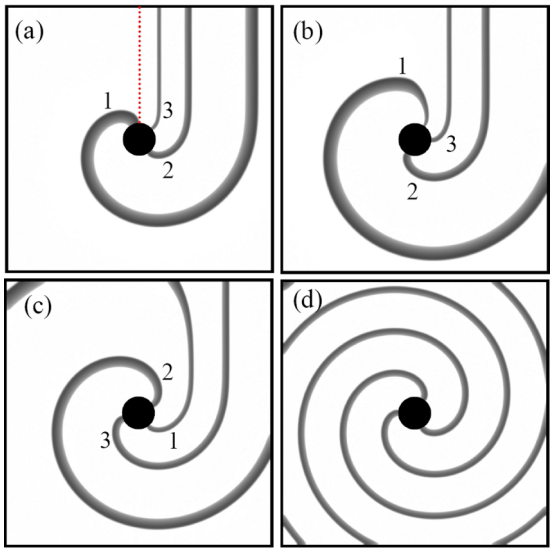

FIG. 5. Dynamics of a three-armed spiral wave pinned to an obstacle with a diameter of 10.0 s.u. in the Oregonator model. (a) Three wave fronts (labeled 1, 2, and 3) are subsequently ignited on the right of the partition (the dashed line). (b) A part of the first arm (1) becomes thinner when it travels into the wake of the third one. (c) Then the second arm (2) becomes the thickest front. (d) Finally, all arms attain the same width and are distributed evenly around the obstacle.

The displacements are plotted with time in Fig. 6(c). The angular velocities of all spiral arms (ω_1, ω_2, and ω_3), shown in Fig. 6(d), are estimated from the local slopes of the lines in the time-space plot.

As found in the experiments, the interaction between adjacent arms results in time-dependent angular velocities ω_1, ω_2, and ω_3, which in turn cause the angular displacements S_{12}, S_{23}, and S_{31} to oscillate in time. In the beginning, each arm has a different velocity depending on the order of initiation: the later the initiation, the slower the propagation. At $t = 0$, ω_1, ω_2, and ω_3 are 116.8, 68.7, and 36.6° t.u.$^{-1}$, respectively, so that the displacement between arm 1 and arm 2 (S_{12}) is larger than that between arm 2 and arm 3 (S_{23}).

The temporal dynamics of the displacement S_{12} are affected by the velocities ω_1 and ω_2 as follows. When the measurement starts S_{12} increases, since the first arm rotates faster than the second one ($\omega_1 > \omega_2$). Shortly after the first arm passes the partition location (at $t = 0.7$) and propagates into the wake of the third arm, its velocity ω_1 rapidly decreases while the velocity of the second arm ω_2 continually increases. At $t = 1.0$, ω_1 and ω_2 approach the same value so that S_{12} reaches a local maximum. After that, ω_1 is smaller than ω_2 and S_{12} decreases. ω_1 reaches a minimum at $t = 2.0$ before it becomes larger until it equals ω_2 at $t = 4.0$ where S_{12} decreases to a minimum. From this time on, the first arm rotates again faster than the second arm ($\omega_1 > \omega_2$), so that S_{12} continually increases to a maximum at $t = 10.0$. Then the oscillations of ω_1, ω_2, and S_{12} keep going while their amplitudes decrease in time.

Similar to S_{12}, the displacements S_{23} and S_{31} are affected by the corresponding velocities, i.e., ω_2 and ω_3 (for S_{23}) or ω_3 and ω_1 (for S_{31}). All displacements S_{12}, S_{23}, and S_{31} and velocities

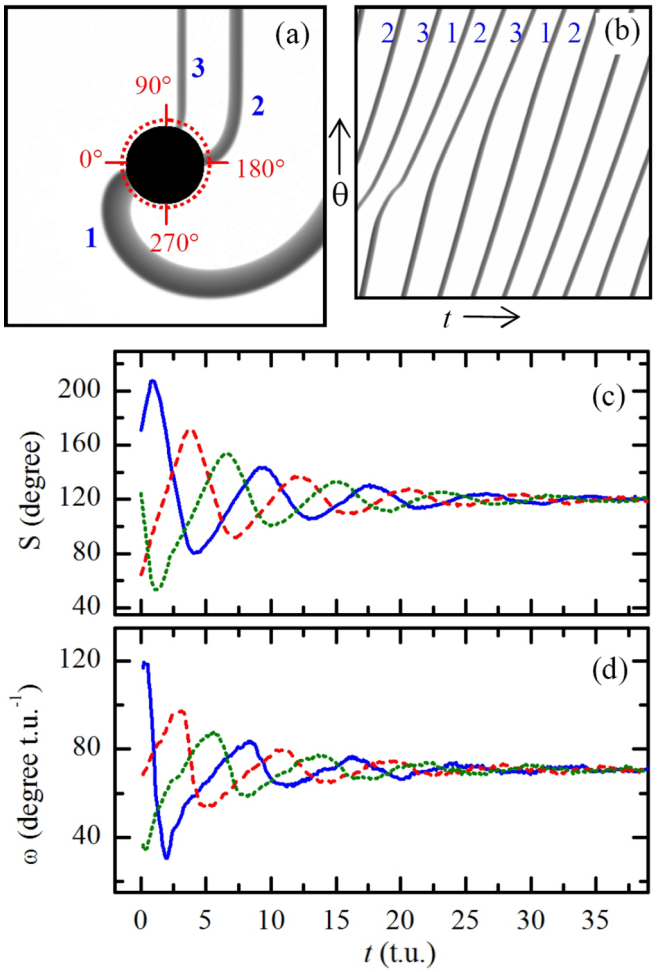

FIG. 6. Dynamics of the three-armed spiral wave in the simulations. (a) Pixels along the dashed circle are taken to create (b) a time-space plot. The spiral arms are labeled 1, 2, and 3 with respect to the initiation order. (c) The angular displacements between adjacent spiral arms S_{12}, S_{23}, and S_{31} (solid, dashed, and dotted lines, respectively) and (d) the angular velocities of the spiral arms ω_1, ω_2, and ω_3 (solid, dashed, and dotted lines, respectively) are plotted as a function of time.

ω_1, ω_2, and ω_3 continually oscillate with gradually damped amplitudes. After $t = 40$ [not shown in Figs. 6(c) and 6(d)] all arms are distributed evenly around the obstacle with the displacement of $120.0^\circ \pm 0.5^\circ$ and propagate with velocity of 70.8° t.u.$^{-1} \pm 0.6^\circ$ t.u.$^{-1}$.

Wave periods of the spiral arms close to the obstacle $T_{\rm obs}$ are derived from the time-space plot [Fig. 6(b)] using the same method as in the experimental results. The wave periods $T_{1\rm obs}$, $T_{2\rm obs}$, and $T_{3\rm obs}$ of all spiral arms in Fig. 7(a) oscillate with damped amplitudes similar to their corresponding angular velocities ω_1, ω_2, and ω_3 [Fig. 6(d)], and the velocity increases monotonously with the wave period [Fig. 7(b)] as found in the experimental part. These results show that the damped oscillations of the displacements [Fig. 6(c)] and wave velocities [Fig. 6(d)] originate from the oscillation of the wave periods of all spiral arms and the dispersion relation.

We perform a further analysis of the temporal dynamics of the angular displacements [in Fig. 6(c)] of the simulated

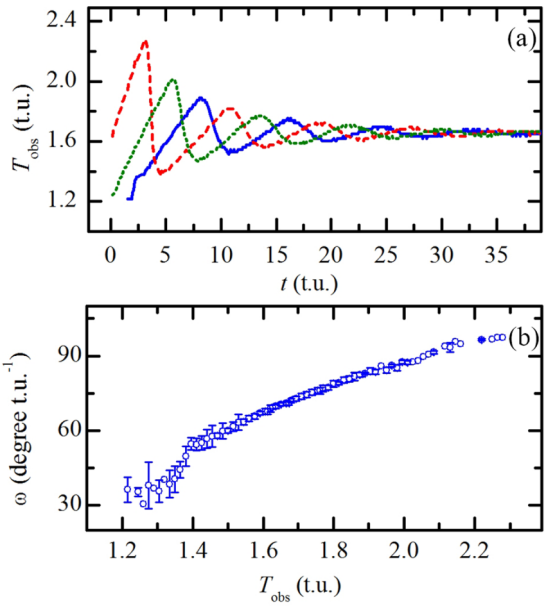

FIG. 7. (a) Time-dependent wave periods close to the obstacle $T_{\rm obs}$ of the spiral arms 1, 2, and 3: $T_{1\rm obs}$, $T_{2\rm obs}$, and $T_{3\rm obs}$ (solid, dashed, and dotted lines, respectively) and (b) dispersion relation of the three-armed spiral wave in the simulations. Circles represent the average value of measured angular velocities corresponding to a given wave period; standard deviation indicated by bars.

multiarmed spiral wave by fitting to an underdamped harmonic oscillation:

$$S = S_0 + Ae^{-at}\sin[2\pi(t - t_0)/w], \tag{2}$$

where S is the angular displacement, S_0 the offset, A the oscillation amplitude, α the damping parameter, t_0 the starting time, and w the oscillation period. As shown in Fig. 8, the function fits well with the displacements in Fig. 6(c) when the parameter values are as follows: $S_0 = 120^\circ$ and $w = 8.4$ for all S_{12}, S_{23}, and S_{31}, while $A = 87.8^\circ$, 63.1°, and 75.4°; $\alpha = 0.146$, 0.107, and 0.128; and $t_0 = -1.25$, 1.62, and 4.17 for S_{12}, S_{23}, and S_{31}, respectively.

We now consider the wave dynamics far from the obstacle. As in the experiments, we perform additional simulations on single-armed and two-armed spiral waves to investigate the effect of the number of arms on the wave period far from the obstacles. The wave period is measured at the left bottom corner of the systems. Similar to the experimental results in Fig. 4, the wave periods change monotonously at the beginning and approach stationary values, as shown in Fig. 9. An increment of the number of arms results in a decrease of the wave period. For the single-armed, two-armed, and three-armed spiral waves, we find their periods $T_1 = 2.97$, $T_2 = 2.03$, and $T_3 = 1.71$ t.u., respectively. Each spiral arm completes one revolution within an interval prolonged by the number of arms: $T_1 = 2.97$, $2T_2 = 4.06$, and $3T_3 = 5.13$ t.u., and wave velocities are 12.12, 9.23, and 7.66 s.u. t.u.$^{-1}$ for one, two, and three arms, respectively. Thus, the wave interaction slows the rotation of spiral arms, as found in the experiments.

Finally, we perform simulations with more arms in order to study the effect of the spiral arm number on the wave dynamics. To complete the wave initiation using the same

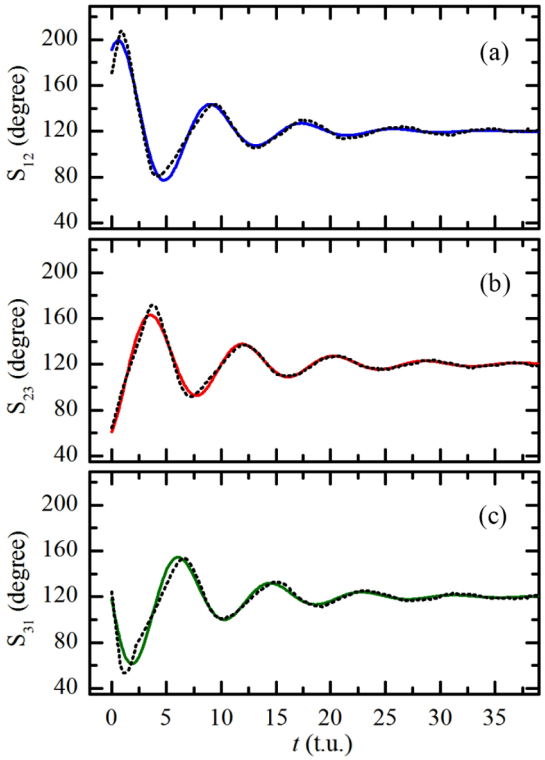

FIG. 8. Fitting of the angular displacements to an underdamped harmonic oscillation [Eq. (2)]: (a) S_{12}, (b) S_{23}, and (c) S_{31}. Solid and dotted lines depict the results from the functions and from the simulations, respectively.

method, the obstacle needs to be enlarged from 10.0 s.u. to 15.0, 21.0, and 250 s.u. for four, five, and six arms, respectively. In all cases, we observe typical damped oscillations similar to those of three-armed spiral waves. Therefore, we expect that the damped oscillation dynamics are generic for pinned multiarmed spiral waves initiated by multiple stimuli as in this study.

IV. DISCUSSION AND CONCLUSION

We have presented a study of the dynamics of multiarmed spiral waves pinned to an obstacle in the Belousov-Zhabotinsky reaction as well as in simulations with

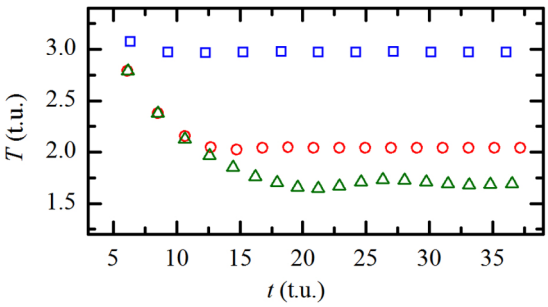

FIG. 9. The wave period of multiarmed spiral waves in the Oregonator model, measured far from the obstacle (i.e., at the left bottom corner in Fig. 5). Squares, circles, and triangles depict the period of single-armed, two-armed, and three-armed spiral waves, respectively.

the Oregonator model. To generate the multiarmed spiral waves, wave fronts are initiated by a series of wave stimuli close to a single partition located between an inner wall and the boundary of the obstacle. The spiral arms interact with each other via the refractory tail created by preceding waves.

Close to the obstacle boundary, an intricate dynamics of the multiarmed spiral waves is observed. As a result of the interaction between spiral arms, the arms initiated later have at the beginning a lower angular velocity. Subsequently, all angular velocities oscillate with some phase shifts, i.e., they reach local minima and maxima at different times. This temporal dynamics of angular velocities causes angular displacements between adjacent arms to oscillate with phase shifts too. In the course of time, the oscillating amplitudes of all angular velocities and those of angular displacements decay until they reach stationary values. The simulated data allow a further interpretation of this temporal evolution of angular displacements as underdamped harmonic oscillations. During the adjustment of the displacements, the wave periods also oscillate with damped amplitudes. Beside the oscillations, the velocities increase monotonously with the wave periods.

It is well known that the propagation of sequential wave fronts obey the dispersion relation in which the wave velocity is a hyperbolic tangent function of the wave period [24]. As a result, multiple wave fronts created from a series of stimuli reach a given position with wave period and velocity monotonously decreasing in time. In this study, the pinned fronts evolve at obstacles as "reentrant waves" (the fronts revisit the positions that they have previously passed). In contrast to multiple plane waves [23,24], the wave periods close to the obstacles of these reentrant waves do not monotonously decrease in time but they oscillate with decreasing amplitude. The oscillations of the wave periods, in turn, generate damped oscillations of the wave velocities and the displacements.

The presented dynamics of pinned waves close to obstacles are similar to a uniform traffic flow in simulations of cars on a single circular path [28]. In such a case, all cars have the same velocity and are equally distributed when the velocity of each individual car is set properly, e.g., as a hyperbolic tangent function [28] of its headway (distance of the car and its preceding one). The final state of the pinned waves presented here looks similar to that of a propagating chemical wave train in a thin ring-shaped reaction field, where the uniformed distribution of waves is developed via a monotonously relaxation [29].

It has been shown that multiarmed spiral waves are stabilized by pinning to obstacles [17,18], but after the obstacles (i.e., a Cl^- droplet in Ref. [17] and a laser spot in Ref. [18]) are removed, the spiral arms separate and rotate around individual centers and subsequently interact with each other. In the presence of the obstacle, we expect that complicated interactions of the multiarmed spiral waves may occur when they are forced to be temporally unpinned (the wave ends alternately detached and reattached to the obstacle [27]).

We expect an important impact of multiarmed pinned spiral waves on the dynamics of excitable media, e.g., the Belousov-Zhabotinsky reaction, slime mold colonies, or cardiac systems. Obstacles are found to stabilize rotating spiral waves even in media subject to gradients [5], and the pinned waves are released from the obstacles only under a sufficiently strong

external forcing [13–16]. On the other hand, multiarmed spiral waves have a frequency increasing with the number of arms [30]. Multiarmed spiral waves pinned to obstacles would act as high-frequency sources of excitation, which are robust against perturbations and thus result potentially in quite severe pathological conditions when they occur in the heart. Therefore, it is important to elucidate the dynamical features as well as the conditions for eliminating multiarmed spiral waves by external perturbations, e.g., wave trains [13,14] or electrical forcing [15,16].

ACKNOWLEDGMENTS

We thank the Department of Physics, Faculty of Science, the Research and Development Institute (KURDI), the Center for Advanced Studies of Industrial Technology, the Science Achievement Scholarship of Thailand (SAST), the Graduate School, Kasetsart University, and the Office of the Higher Education Commission and King Mongkut's University of Technology North Bangkok (Contract No. KMUTNB-NRU-59-05) for financial support.

[1] S. Nettesheim, A. von Oertzen, H. H. Rotermund, and G. Ertl, Reaction diffusion patterns in the catalytic CO-oxidation on Pt(110): Front propagation and spiral waves, J. Chem. Phys. **98**, 9977 (1993).

[2] F. Siegert and C. Weijer, Digital image processing of optical density wave propagation in *Dictyostelium discoideum* and analysis of the effects of caffeine and ammonia, J. Cell Sci. **93**, 325 (1989).

[3] J. Lechleiter, S. Girard, E. Peralta, and D. Clapham, Spiral calcium wave propagation and annihilation in *Xenopus laevis* oocytes, Science **252**, 123 (1991).

[4] A. T. Winfree, Spiral waves of chemical activity, Science **175**, 634 (1972).

[5] J. M. Davidenko, A. M. Pertsov, R. Salomonz, W. Baxter, and J. Jalife, Stationary and drifting spiral waves of excitation in isolated cardiac muscle, Nature (London) **355**, 349 (1992).

[6] A. T. Winfree, Electrical turbulence in three-dimensional heart muscle, Science **266**, 1003 (1994).

[7] E. M. Cherry and F. H. Fenton, Visualization of spiral and scroll waves in simulated and experimental cardiac tissue, New J. Phys. **10**, 125016 (2008).

[8] J. J. Tyson and J. P. Keener, Singular perturbation theory of traveling waves in excitable media, Physica D **32**, 327 (1988).

[9] Y. Q. Fu, H. Zhang, Z. Cao, B. Zheng, and G. Hu, Removal of a pinned spiral by generating target waves with a localized stimulus, Phys. Rev. E **72**, 046206 (2005).

[10] Z. Y. Lim, B. Maskara, F. Aguel, R. Emokpae, and L. Tung, Spiral wave attachment to millimeter-sized obstacles, Circulation **114**, 2113 (2006).

[11] O. Steinbock and S. C. Müller, Chemical spiral rotation is controlled by light-induced artificial cores, Physica A **188**, 61 (1992).

[12] M. Sutthiopad, J. Luengviriya, P. Porjai, M. Phantu, J. Kanchanawarin, S. C. Müller, and C. Luengviriya, Propagation of spiral waves pinned to circular and rectangular obstacles, Phys. Rev. E **91**, 052912 (2015).

[13] M. Tanaka, A. Isomura, M. Hörning, H. Kitahata, K. Agladze, and K. Yoshikawa, Unpinning of a spiral wave anchored around a circular obstacle by an external wave train: Common aspects of a chemical reaction and cardiomyocyte tissue, Chaos **19**, 043114 (2009).

[14] M. Tanaka, M. Hörning, H. Kitahata, and K. Yoshikawa, Elimination of a spiral wave pinned at an obstacle by a train of plane waves: Effect of diffusion between obstacles and surrounding media, Chaos **25**, 103127 (2015).

[15] M. Sutthiopad, J. Luengviriya, P. Porjai, B. Tomapatanaget, S. C. Müller, and C. Luengviriya, Unpinning of spiral waves by electrical forcing in excitable chemical media, Phys. Rev. E **89**, 052902 (2014).

[16] P. Porjai, M. Sutthiopad, J. Luengviriya, M. Phantu, S. C. Müller, and C. Luengviriya, Electrically forced unpinning of spiral waves from circular and rectangular obstacles, Chem. Phys. Lett. **660**, 283 (2016).

[17] K. I. Agladze and V. I. Krinsky, Multi-armed vortices in an active chemical medium, Nature (London) **296**, 424 (1982).

[18] O. Steinbock and S. C. Müller, Multi-armed spirals in a light-controlled excitable reaction, Int. J. Bif. Chaos **03**, 437 (1993).

[19] B. Vasiev, F. Siegert, and C. J. Weijer, Multiarmed Spirals in Excitable Media, Phys. Rev. Lett. **78**, 2489 (1997).

[20] T. J. Wu, M. A. Bray, C. T. Ting, and S. F. Lin, Stable bound pair of spiral waves in rabbit ventricles, J. Cardiovasc. Electrophysiol. **13**, 414 (2002).

[21] N. Bursac, F. Aguel, and L. Tung, Multiarm spirals in a two-dimensional cardiac substrate, Proc. Natl. Acad. Sci. USA **101**, 15530 (2004).

[22] R. J. Field and R. M. Noyes, Oscillations in chemical systems. IV. Limit cycle behavior in a model of a real chemical reaction, J. Chem. Phys. **60**, 1877 (1974).

[23] H. Sevcikova and M. Marek, Comparison of dispersion relations for propagating waves in the Belousov-Zhabotinsky reaction, Physica D **39**, 15 (1989).

[24] J. M. Flesselles, A. Belmonte, and V. Gaspar, Dispersion relation for waves in the Belousov-Zhabotinsky reaction, J. Chem. Soc. Faraday Trans. **94**, 851 (1998).

[25] W. Jahnke and A. T. Winfree, A survey of spiral-wave behaviors in the Oregonator model, Int. J. Bif. Chaos **01**, 445 (1991).

[26] M. Dowle, R. M. Mantel, and D. Barkley, Fast simulations of waves in three-dimensional excitable media, Int. J. Bif. Chaos **07**, 2529 (1997).

[27] J. Luengviriya, M. Sutthiopad, M. Phantu, P. Porjai, J. Kanchanawarin, S. C. Müller, and C. Luengviriya, Influence of excitability on unpinning and termination of spiral waves, Phys. Rev. E **90**, 052919 (2014).

[28] M. Bando, K. Hasebe, A. Nakayama, A. Shibata, and Y. Sukiyama, Dynamical model of traffic congestion and numerical simulation, Phys. Rev. E **51**, 1035 (1995).

[29] N. J. Suematsu, T. Sato, I. N. Motoike, K. Kashima, and S. Nakata, Density wave propagation of a wave train in a closed excitable medium, Phys. Rev. E **84**, 046203 (2011).

[30] R. M. Zaritski, J. Ju, and I. Ashkenazi, Spontaneous formation of multiarmed spiral waves in various simple models of weakly excitable media, Int. J. Bif. Chaos **15**, 4087 (2005).